

Retrospective Study

Contrast-enhanced multidetector computed tomography features and histogram analysis can differentiate ameloblastomas from central giant cell granulomas

Adarsh Ghosh, Meyyappan Lakshmanan, Smita Manchanda, Ashu Seith Bhalla, Prem Kumar, Ongkila Bhutia, Asit Ranjan Mridha

Specialty type: Radiology, nuclear medicine and medical imaging

Provenance and peer review: Invited article; Externally peer reviewed.

Peer-review model: Single blind

Peer-review report's scientific quality classification

Grade A (Excellent): 0
Grade B (Very good): 0
Grade C (Good): C, C
Grade D (Fair): 0
Grade E (Poor): 0

P-Reviewer: Chen Q, China; Xie Q, China

Received: March 19, 2022

Peer-review started: March 19, 2022

First decision: June 16, 2022

Revised: July 5, 2022

Accepted: September 2, 2022

Article in press: September 2, 2022

Published online: September 28, 2022



Adarsh Ghosh, Department of Radiology, Children's Hospital of Philadelphia, Philadelphia, PA 19104, United States

Meyyappan Lakshmanan, Smita Manchanda, Department of Radiology, All India Institute of Medical Sciences, New Delhi 110029, India

Ashu Seith Bhalla, Department of Radiodiagnosis, All India Institute of Medical Sciences, New Delhi 110029, India

Prem Kumar, Ongkila Bhutia, Department of Oral & Maxillofacial Surgery, All India Institute of Medical Sciences, New Delhi 110029, India

Asit Ranjan Mridha, Department of Pathology, All India Institute of Medical Sciences, Ansari Nagar, New Delhi 110029, India

Corresponding author: Ashu Seith Bhalla, MD, Professor, Department of Radiodiagnosis, All India Institute of Medical Sciences, New Delhi 110029, India. ashubhalla1@yahoo.com

Abstract

BACKGROUND

No qualitative or quantitative analysis of contrast-enhanced computed tomography (CT) images has been reported for the differentiation between ameloblastomas and central giant cell granulomas (CGCGs).

AIM

To describe differentiating multidetector CT (MDCT) features in CGCGs and ameloblastomas and to compare differences in enhancement of these lesions qualitatively and using histogram analysis.

METHODS

MDCT of CGCGs and ameloblastomas was retrospectively reviewed to evaluate qualitative imaging descriptors. Histogram analysis was used to compare the extent of enhancement of the soft tissue. Fisher's exact tests and Mann-Whitney *U* test were used for statistical analysis ($P < 0.05$).

RESULTS

Twelve CGCGs and 33 ameloblastomas were reviewed. Ameloblastomas had a predilection for the posterior mandible with none of the CGCGs involving the angle. CGCGs were multilocular (58.3%), with a mixed lytic sclerotic appearance (75%). Soft tissue component was present in 91% of CGCGs, which showed hyperenhancement (compared to surrounding muscles) in 50% of cases, while the remaining showed isoenhancement. Matrix mineralization was present in 83.3% of cases. Ameloblastomas presented as a unilocular (66.7%), lytic (60.6%) masses with solid components present in 81.8% of cases. However, the solid component showed isoenhancement in 63%. No matrix mineralization was present in 69.7% of cases. Quantitatively, the enhancement of soft tissue in CGCG was significantly higher than in ameloblastoma on histogram analysis ($P < 0.05$), with a minimum enhancement of > 49.05 HU in the tumour providing 100% sensitivity and 85% specificity in identifying a CGCG.

CONCLUSION

A multilocular, lytic sclerotic lesion with significant hyperenhancement in soft tissue, which spares the angle of the mandible and has matrix mineralization, should indicate prospective diagnosis of CGCG.

Key Words: Ameloblastoma; Granuloma; Giant cell; Multidetector CT

©The Author(s) 2022. Published by Baishideng Publishing Group Inc. All rights reserved.

Core Tip: Central giant cell granulomas (CGCGs) are rare tumours of the jaw. This study evaluated the findings of CGCGs on contrast-enhanced computed tomography in contrast with ameloblastomas, which are the most common tumours of the jaw in the developing world.

Citation: Ghosh A, Lakshmanan M, Manchanda S, Bhalla AS, Kumar P, Bhutia O, Mridha AR. Contrast-enhanced multidetector computed tomography features and histogram analysis can differentiate ameloblastomas from central giant cell granulomas. *World J Radiol* 2022; 14(9): 329-341

URL: <https://www.wjgnet.com/1949-8470/full/v14/i9/329.htm>

DOI: <https://dx.doi.org/10.4329/wjr.v14.i9.329>

INTRODUCTION

The most current World Health Organization classification of jaw tumours places giant cell granulomas under “giant cell lesions and simple bone cyst”. These include both central and peripheral giant cell granulomas[1]. Central giant cell granuloma (CGCG) usually appears as an expansile, multiloculated lesion with post-contrast enhancement and soft tissue extension[2-4]. Histologically it is characterized by focally distributed giant cells, spindle cells and possible areas of haemorrhage. A similar radiological and histopathological appearance may also be seen in brown tumours of hyperparathyroidism, and further clinical and laboratory correlation is required whenever aggressive, atypical or multiple CGCGs are seen[1,5]. CGCGs are slow-growing and insidious, although, increased rates of growth, presence of pain, tooth resorption or cortical erosions are considered signs of aggressive behaviour[2,3,6]. CGCGs are rare and tend to occur with a female preponderance in the second decade of life. Accelerated growth during pregnancy or following childbirth suggests hormone responsiveness of CGCGs. Although the exact pathophysiology of the tumour is yet to be elucidated: a reparative response to trauma, haemorrhagic products and inflammation is presumed to result in tumorigenesis. The classical lytic multilocular appearance of CGCGs on radiographs makes difficult their differentiation from ameloblastomas, odontogenic cyst, aneurysmal bone cysts, and odontogenic fibromas[3,7]. This differentiation is, however, vital because CGCGs are treated less aggressively (curettage, intralesional interferon, steroids or calcitonin injections[8]) as compared to other lesions with a similar radiological appearance. Ameloblastomas are by far the most prevalent odontogenic tumour in the developing world[9], constituting about 14% of all jaw lesions[10]. Although benign, ameloblastomas exhibit an aggressive growth pattern, with up to 70% of cases[11] undergoing malignant transformation. It presents most frequently in males, in their third to fifth decades of life, as a slowly progressive swelling. The lesion favours the posterior mandible (63.15% of all cases as per one study[12]) and on imaging is a close differential of CGCGs with its unilocular or multilocular, lytic, expansive appearance[13]. Ameloblastomas are treated more radically and aggressively (with block resection, radiotherapy and vemurafenib[14]) vis-à-vis CGCGs making differentiation between the two crucial clinically.

Contrast-enhanced computed tomography (CT) can help characterise tumour biology better than noncontrast scans[15]. Although tumour location, appearance, contour and mass effect of the lesion on surrounding structures and teeth can be easily evaluated on noncontrast multidetector CT (MDCT)[4,7,16,17] or on cone beam CT (CBCT), the presence of enhancing soft tissue and the extent of enhancement in the tumour can provide significant insight into tumour biology and can differentiate tumour types and pathological processes. For example, contrast-enhanced CT (CECT) helps differentiate purely cystic lesions of the jaw from cyst like lesions[18], a task relatively difficult on noncontrast MDCT or CBCT. Similarly, contrast-enhanced dynamic MDCT can help differentiate ameloblastomas[19] from other cystic jaw lesions, including keratocystic odontogenic tumours. Further quantification of the extent of tumour enhancement using histogram and texture analysis[20] can also characterise these tumours. However, to our knowledge, no qualitative or quantitative analysis of CECT images has been reported for the differentiation between ameloblastomas and CGCGs.

Given this background, we undertook this study to compare the MDCT features of CGCGs and ameloblastomas. More specifically we compared the utility of quantitative and qualitative evaluation of extent of tumour enhancement in differentiation of these two tumours.

MATERIALS AND METHODS

Subjects

The electronic records available from the Department of Pathology were searched to identify cases of CGCGs and ameloblastomas, between December 2016 and January 2019. All cases with MDCT images were included in the study, and six patients who did not have MDCT images were excluded. A total of 12 CGCGs and 33 ameloblastomas were identified and used in this study. The study was approved by the Institutional Ethics Committee (Ref No: IEC-622/03.07.2020, RP-31/2020).

Imaging technique

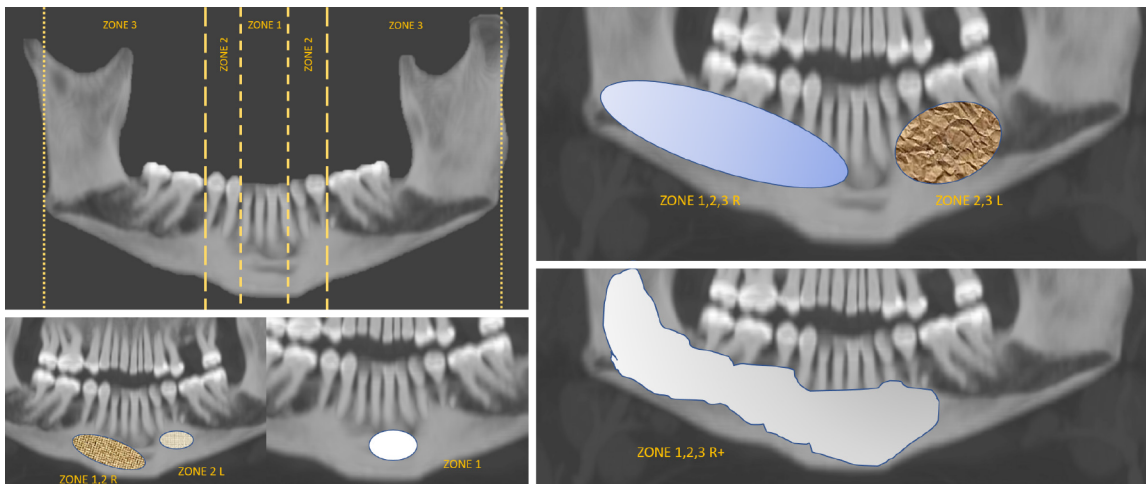
All MDCT acquisitions were performed either on a 64-MDCT scanner (Siemens SOMATOM Sensation, Erlangen, Germany) or 128-MDCT scanner (Siemens SOMATOM Definition Flash) available in our department. The images were acquired using 120 kV with automated tube current modulation, and a quality reference mAs of 80. A slice thickness of 0.6 mm was used. A 16-cm field of view, 512 × 512 matrix, was used to reconstruct data with routine 1mm sections being obtained using standard soft tissue and bone window kernels. CECT images were available for 38 of these 45 scans. Among these 38, venous phase images acquired at 60–70 s after intravenous injection were available in 35 patients (8 CGCGs and 27 ameloblastomas) [1–1.5 mL/kg of nonionic iodinated contrast (Iohexol 350 mg iodine/mL)]. Only arterial phase images were available as part of a head and neck angiography protocol in three patients. Noncontrast MDCT was available in seven patients.

Imaging interpretation

Two radiologists with 16 and 6 years' experience in head and neck imaging, blinded to clinical and pathological data reviewed all the MDCT scans in consensus. Nonconsensus was resolved by reviewing with a third radiologist. Zone-wise mapping of each lesion was done, as explained in Figure 1. Location of the lesion (mandible or maxilla); density (mixed, lytic or sclerotic as characterized on the bone window); multilocularity (unilocular with 1 or 2 thin septae; multilocular, honeycombing pattern); presence or absence of solid components; and erosion or thinning of the surrounding cortex were recorded. In mandibular lesions, the involvement of the angle (yes/no), and the status of the inferior alveolar canal was recorded (involvement/erosion) as well. The status of the overlying teeth (missing or root resorbed/present/adjoining roots displaced), and adjacent fat stranding and muscle thickening (present or absent) were noted. Venous phase images were evaluated ($n = 35$) to quantify the amount of soft tissue in each lesion (0–10%, 10%–25%, 25%–50%, 50%–75% and > 75%) and the type of enhancement of the solid component in the lesion were also characterised (purely cystic, hypoenhancing, isoenhancing, or hyperenhancing – the enhancement in these cases was compared to that of the surrounding muscles). Mineralisation of the tumour was recorded (absent, mineralised osteoid, thin bony septa, or thick septa with associated matrix). The three largest diameters of each lesion were recorded (along and perpendicular to the axis of mandible, and craniocaudal). These measurements were then used to derive the lesion's volume using the volume formula for an ellipsoid ($0.523 \times AP \times TR \times CC$).

Quantitative analysis of enhancement

The venous phase MDCT images were evaluated to compare the degree of enhancement between the tumours. Specifically, the contrast-enhanced MDCT images were opened on 3D Slicer 4.11.0 (<https://download.slicer.org/>). A freehand oval region of interest (ROI) measuring at least 1 cm in diameter was drawn on the largest bulk of the tumour, ensuring that the ROI was placed on soft tissue only, avoiding bony septa (Supplementary Figure 1). This was done by AG with 6 years' experience in



DOI: 10.4329/wjr.v14.i9.329 Copyright ©The Author(s) 2022.

Figure 1 Location of every lesion was classified into the following zones: 1, limited to the incisors; 2, limited to the canine and premolars; and 3, limited to the molars and posterior mandible. A similar classification was applied to the maxilla. Lesions extending over multiple zones were classified as such, and a suffix of R or L was used to denote right or left-sided location. When the lesion crossed the midline across multiple zones, + was used to denote the same.

head and neck imaging and ROI placement was reviewed by SM. The pyRadiomics plugin (<https://pyradiomics.readthedocs.io/en/Latest/index.html>) was used to evaluate the histogram of the distribution of the HUs in the ROIs. Skewness, uniformity, entropy, kurtosis, and mean, median, maximum, minimum, 10th and 90th percentiles of the HU values in the histogram were evaluated. Purely cystic lesions ($n = 6$) were excluded from this analysis.

Statistical analysis

All data were tabulated and tested for normality when indicated. Continuous data were compared between the two data sets using the Mann–Whitney U test, while Fisher’s exact test was used to compare categorical data. $P < 0.05$ was considered statistically significant. Receiver operating characteristic (ROC) curve analysis was used to obtain the area under the curve (AUC) for texture parameters found to be significantly different between the two groups. Optimal cutoffs were obtained using bootstrapped Youden index. A leave-one-out cross-validation of the various enhancement parameters was done to evaluate generalisability.

RESULTS

A total of 12 CGCGs and 33 ameloblastomas were included in our study. The median age of patients with ameloblastoma was higher [35 years [95% confidence interval (CI) 28–48 years] as compared to patients with CGCG [29 years (95% CI 18–42 years)]; however, this was not significant ($P = 0.26$). Of the patients having ameloblastomas, 27.30% ($n = 9$) were female and 72.70% ($n = 24$) were male. The prevalence of CGCGs was nearly equal between the sexes: 41.70% ($n = 5$) in females *versus* 58.30% ($n = 7$) in males. This difference was again not significant.

Location

Both the pathologies favoured the mandible, with five ameloblastomas and four CGCGs appearing in the maxilla. CGCGs favoured a more central location with six lesions being located in zone 1 (50.00%), three in zone 2 (25.00%) and two in zone 3 (16.70%) (Table 1 and Figure 1). Only a single CGCG was large enough to involve zones 1, 2 and 3 simultaneously. This was significantly ($P < 0.0001$) different from ameloblastomas, which had a more varied distribution. Fourteen (42.40%) ameloblastomas were located exclusively in zone 3. Simultaneously, nine ameloblastomas were large enough to involve all three zones and two were large enough to cross the midline. Fifty per cent ($n = 14$ out of 28) of ameloblastomas had involvement of the angle of the mandible. In contrast, none of the CGCGs had this feature ($P = 0.013$).

Volume and size

Lesion volume was determined using the ellipsoid formula. CGCGs were significantly smaller in volume (median 10.31 cm³) as compared to ameloblastomas (median 35.9 cm³) ($P = 0.027$) (Table 2). ROC curve analysis and the associated cutoff are provided in Table 3. While there was considerable overlap

Table 1 Comparison of the various multidetector computed tomography imaging features between ameloblastoma and central giant cell granuloma

MDCT features		Pathology				Fisher's exact test (exact sig. two-sided)
		Ameloblastoma		CGCG		
		Count	% of all cases	Count	% of all cases	
Zone wise location (figure × for reference)	1, 2, 3	9	27.3 (14.4–43.9)	1	8.3 (0.9–32.8)	< 0.0001 ^a
	1	0	0.00%	6	50 (24.3–75.7)	
	1, 2	4	12.1 (4.2–26.3)	0	0.00%	
	2	0	0.00%	3	25 (7.6–52.9)	
	2,3	6	18.2 (8–33.7)	0	0.00%	
	3	14	42.4 (26.8–59.3)	2	16.7 (3.6–43.6)	
Density	Mixed	13	39.4 (24.2–56.4)	9	75 (47.1–92.4)	0.036 ^a
	Lytic	20	60.6 (43.6–75.8)	3	25 (7.6–52.9)	
Multilocularity; 1-Unilocular with 1 or 2 thin septae/2-Multilocular/3-Honeycombing	1	22	66.7 (49.7–80.8)	3	25 (7.6–52.9)	0.047 ^a
	2	8	24.2 (12.2–40.6)	7	58.3 (31.2–82)	
	3	3	9.1 (2.6–22.3)	2	16.7 (3.6–43.6)	
Bucco-lingual expansion	1	33	100.00%	12	100.00%	-
Solid component	Absent	6	18.2 (8–33.7)	1	8.3 (0.9–32.8)	0.309
	Present	27	81.8 (66.3–92)	11	91.7 (67.2–99.1)	
Cortical erosion	Thinning	1	3 (0.3–13.3)	1	8.3 (0.9–32.8)	1.000
	Erosion	32	97.86.7–99.7)	11	91.7 (67.2–99.1)	
Angle involved (of lesions in mandible)	No	14	50 (32.2–67.8)	8	100.00%	0.013 ^a
	Yes	14	50 (32.2–67.8)	0	0.00%	
Inferior alveolar canal displacement	No	3	14.3 (4.2–33.4)	2	25 (5.6–59.2)	0.597
	Yes	18	85.7 (66.6–95.8)	6	75 (40.8–94.4)	
Status of overlying teeth; Missing-0/Adjoining roots-1/Present-2	0	19	57.6 (40.7–73.2)	8	72.7 (43.5–91.7)	0.152
	1	12	36.4 21.6–53.4)	1	9.1 (1–35.3)	
	2	2	6.1 (1.3–18.1)	2	18.2 (4–46.7)	
Inferior alveolar canal erosion	No	2	9.5 (2–27.2)	3	37.5 (11.9–70.5)	0.112
	Yes	19	90.5 (72.8–98)	5	62.5 (29.5–88.1)	
Adjacent fat stranding	Absent	27	81.8 (66.3–92)	10	83.3 (56.4–96.4)	1.000
	Present	6	18.2 (8–33.7)	2	16.7 (3.6–43.6)	
Adjacent muscle thickening	Absent	26	78.8 (62.8–90)	11	91.7 (67.2–99.1)	0.419
	Present	7	21.2 (10–37.2)	1	8.3 (0.9–32.8)	
Extent of enhancement of soft tissue component in venous phase;	0	6	22.2 (9.8–40.2)	0	0.00%	

0-cystic/1- hypoenhancing/2- isoenhancing/3- hyperenhancing	2	17	63 (44.2–79.1)	4	50 (19.9–80.1)	0.013 ^a
	3	1	3.7 (0.4–16)	4	50 (19.9–80.1)	
	1	3	11.1 (3.2–26.8)	0	0.00%	
Amount of solid component	> 75%	9	33.3 (17.9–52.1)	6	75 (40.8–94.4)	0.061
	0- < 10%	8	29.6 (15.1–48.2)	0	0.00%	
	10%-25%	3	11.1 (3.2–26.8)	0	0.00%	
	25%-50%	5	18.5 (7.4–35.9)	0	0.00%	
	50%-75%	2	7.4 (1.6–21.7)	2	25 (5.6–59.2)	
Matrix mineralisation; Mineralised osteoid-1; Absent- 2; Thick septae with associated matrix-3; Thin bony septa- 4	1	1	3 (0.3–13.3)	3	25 (7.6–52.9)	0.004 ^a
	2	23	69.7 (52.9–83.2)	2	16.7 (3.6–43.6)	
	3	4	12.1 (4.2–26.3)	3	25 (7.6–52.9)	
	4	5	15.2 (6–30.1)	4	33.3 (12.5–61.2)	
Diameter		33	5.1(4.5–6)	12	3.7(2.1–4.8)	0.011 ^a
Volume		33	35.9 (23.05–47.59)	12	10.31 (3.67–59.37)	0.027 ^a

^aStatistically significant.

CGCG: Central giant cell granulomas; MDCT: Multidetector computed tomography.

Table 2 First-order histogram parameters comparing the extent of enhancement seen in the soft tissue component of ameloblastomas and central giant cell granulomas

		Ameloblastoma (n = 21); median (95%CI)	CGCG (n = 8); median(95%CI)	P value
Histogram parameter (n = 29)	Skewness	0.1 (-0.23–0.22)	0.07 (-0.51–0.47)	0.981
	Median (HU)	74.91 (56.97–93.24)	106.21 (95.1–134.52)	0.002
	Maximum (HU)	121.01 (100.11–150.05)	154.2 (133.42–183.09)	0.013
	90 percentile (HU)	95.32 (75.72–113.71)	137.43 (113.91–150.17)	0.001
	Entropy	1.62 (1.57–1.8)	1.5 (1.34–1.98)	0.487
	10 percentile (HU)	53.32 (34.2–71.13)	82.65 (74.86–116.64)	0.002
	Kurtosis	3.11 (2.71–3.54)	3.25 (2.69–4.08)	0.83
	Mean (HU)	74.06 (58.58–91.92)	106.95 (97.48–132.39)	0.002

CGCG: Central giant cell granulomas; CI: Confidence interval; MDCT: Multidetector computed tomography.

between the two volumes, a cutoff $\leq 13.04 \text{ cm}^3$ obtained 84.85% (68.1%–94.9%) specificity in identifying CGCG. Similarly, the diameter of ameloblastomas (measured along the long axis of the mandible) was higher than that of CGCGs with a cut off of $\leq 3.5 \text{ cm}$ (95%CI $\leq 2.1 \text{ cm}$ to $\leq 4.4 \text{ cm}$) providing 50% (95%CI 21.1%–78.9%) sensitivity and 90.91% (95%CI 75.7%–98.1%) specificity in identifying the latter.

Lesion appearance on bone window

60.6% of ameloblastomas were purely lytic (n = 20), as compared to only 25% of CGCGs (n = 3) (P = 0.047). A majority of all CGCGs (75%; n = 9) were predominantly mixed in appearance with both lytic and sclerotic components being present in the lesion. However, only 39.4% of ameloblastomas were mixed in appearance (n = 13). Neither of the tumours was purely sclerotic. Ameloblastomas (n = 22) were predominantly unilocular (66.7%) compared to 58.3% of CGCGs, which were multilocular. Matrix mineralisation in the form of osteoid, thin septa, or thick septa and associated dense matrix, was more common in CGCGs than ameloblastomas, where 70% showed no matrix mineralisation.

Table 3 Area under the curve of the various statistically significant histogram parameters of tumours in differentiating central giant cell granulomas from ameloblastomas

Variable	10 percentile	90 percentile	Mean	Median	Minimum
Area under the ROC curve (AUC)	0.863	0.875	0.863	0.869	0.887
5, 95%CI	0.685 to 0.962	0.699 to 0.968	0.685 to 0.962	0.692 to 0.965	0.714 to 0.974
Associated criterion (HU)	> 71.13	> 106.33	> 91.92	> 93.24	> 49.05
95%CI	> 66.43 to > 96.63	> 82.80 to > 113.71	> 88.68 to > 114.75	> 93.15 to > 110.22	> 48.51 to > 49.05
Sensitivity %	100 (63.1-100.0)	100 (63.1-100.0)	100 (63.1-100.0)	100 (63.1-100.0)	100 (63.1-100.0)
Specificity %	76.19 (52.8-91.8)	66.67 (43.0-85.4)	76.19 (52.8-91.8)	76.19 (52.8-91.8)	85.71 (63.7-97.0)
Leave-one out sensitivity %	100 (63.06-100)	100 (63.06-100)	100 (63.06-100)	100 (63.06-100)	100 (63.06-100)
Leave-one out specificity %	71.43 (47.82-88.72)	47.62 (25.71-70.22)	71.43 (47.82-88.72)	71.43 (47.82-88.72)	80.95 (58.09-94.55)

AUC: Area under the curve; CI: Confidence interval; ROC: Receiver operating characteristic.

Qualitative evaluation of contrast enhancement

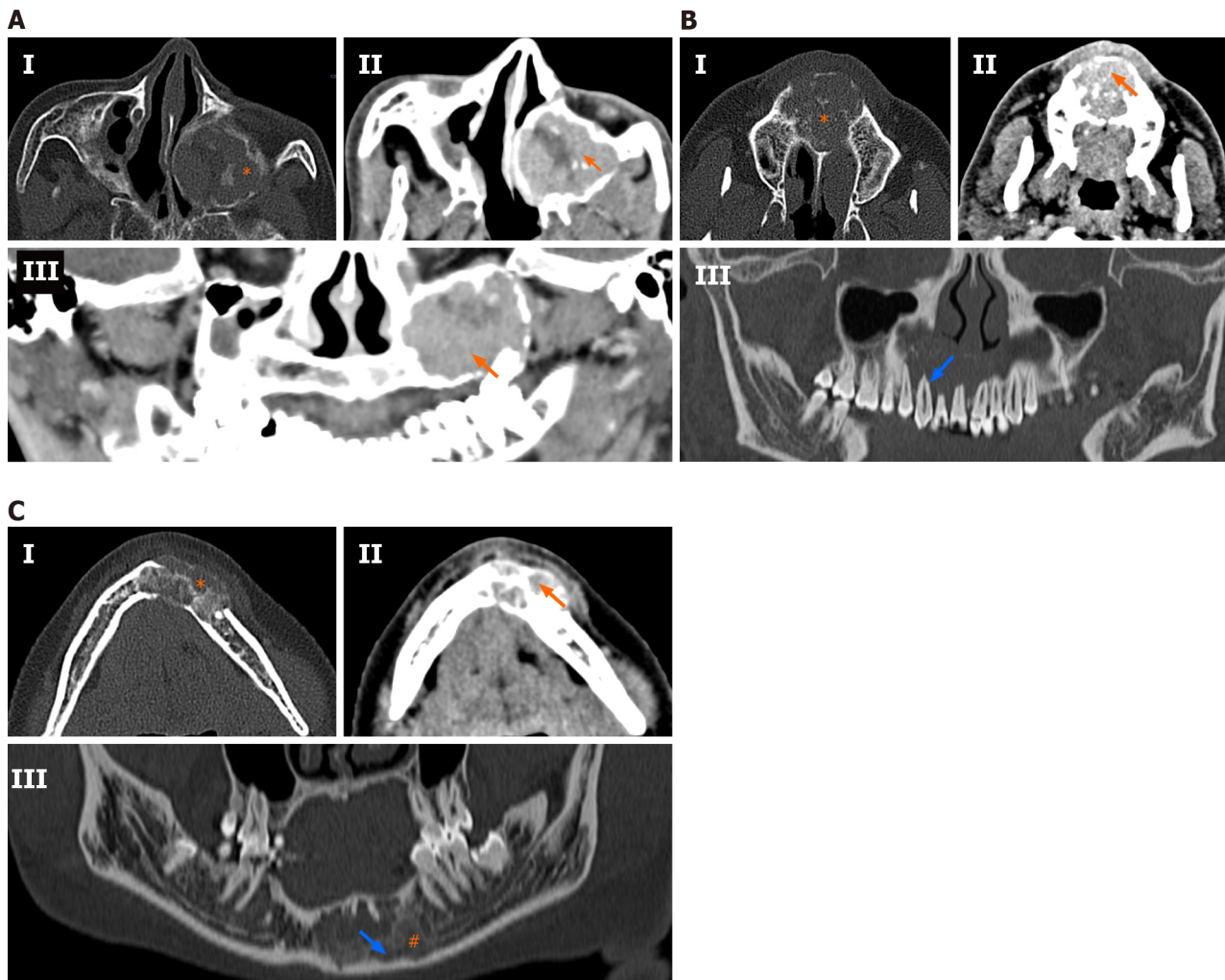
Evaluation of the degree of enhancement of solid component on venous phase images (8 CGCGs and 27 ameloblastomas) showed that six ameloblastomas were purely cystic with no solid component, and 17 (62.9%) ameloblastomas showed enhancement that was similar to the surrounding muscles. In comparison, four (50%) CGCGs showed enhancement higher than the surrounding muscles. This was significantly different ($P = 0.013$) from ameloblastomas, with only one ameloblastoma (3.7%) showing enhancement higher than muscles. These above findings are summarised in [Table 1](#) and [Figure 2](#).

Quantitative evaluation of enhancement

Histogram analysis (8 CGCGs and 21 ameloblastomas) of the enhancement of the solid component in the venous phase image was carried out after excluding the purely cystic lesions ($n = 6$). CGCGs had higher minimum, median, mean and maximum enhancement as compared to ameloblastomas ($P < 0.05$) on venous imaging ([Table 2](#)). A boot-strapped ROC curve analysis provided the AUC of the individual parameters as well as the optimum cutoffs. Minimum enhancement of > 49.0538 , had a sensitivity of 100% and a specificity of 85.71% in identifying a CGCC over ameloblastoma. The cutoffs, their associated sensitivity and specificity, and accuracy metrics of a leave-one-out cross-validation are provided in [Table 3](#).

DISCUSSION

We described the MDCT imaging features of CGCGs and contrasted them with ameloblastomas. Morphologically, both CGCGs and ameloblastomas had several overlapping features – making their differentiation difficult. Both ameloblastomas and CGCGs can be either unilocular or multilocular. Cortical expansion, cortical perforation, root displacement and root resorption are features suggestive of an aggressive variant of CGCG; however, these features are also present in ameloblastomas. MDCT or CBCT is preferred over radiography because it allows better evaluation of the bony anatomy, especially the integrity of the buccal and lingual cortex. MDCT with intravenous contrast allows better evaluation of the soft tissue component in these lesions. Location wise, we found that, although the CGCGs favoured the central jaw, up to 25% of the lesions were also found in the ramus[21,22]. Because of the small size of CGCGs, only one lesion was large enough to involve all the three zones. Ameloblastomas because of their larger sizes tended to involve more than one zone, with the most predominant preference for zone 3 (ramus of the mandible). This varied distribution is similar to that described in the literature[14,15]; involvement of the angle when present was highly specific for ameloblastoma. None of the CGCGs demonstrated the involvement of the angle. CGCGs were considerably smaller ($28.82 \pm 40.75 \text{ cm}^3$) in volume as compared to ameloblastomas ($66.18 \pm 84.33 \text{ cm}^3$) ([Tables 2 and 3](#)). Ameloblastomas are locally aggressive tumours, while CGCGs are slow-growing insidious masses that are sometimes known to regress spontaneously. Thus, the smaller volume of CGCG may be in keeping with the natural history of CGCGs ([Table 2](#)). Cortical expansion, cortical perforation, root displacement and root resorption as previously stated, can occur in both tumours[19,24-26]. Even in our series, there was no difference in the prevalence of root resorption, tooth displacement, cortical expansion or cortical perforation between the two entities ([Table 1](#)). CGCGs were predominantly multilocular (58.3%) with a unilocular appearance in only 25% of cases. In contrast, 67% of ameloblastomas were unilocular. Seventy-five percent of CGCGs



DOI: 10.4329/wjr.v14.i9.329 Copyright ©The Author(s) 2022.

Figure 2 Spectrum of multidetector computed tomography findings in central giant cell granulomas. A: 35-year-old woman presented with upper facial pain and nasal obstruction. Cone beam computed tomography (CBCT) shows a left-sided unilocular lytic lesion arising from the left maxilla (Panel I: Bone window) with compression of the maxillary sinus. Mineralised matrix was scattered in the substance of the tumour (asterisk). The lesion showed a significant soft tissue component, which enhanced to an extent greater than the surrounding muscles [arrow, Panel II and III: Axial and curved multiplanar reconstructed (MPR) coronal soft tissue images]. Hyperenhancement of the soft tissue tumour component was highly suggestive of a prospective central giant cell granuloma (CGCG) diagnosis; B: A 30-year-old man presented with pain and upper jaw swelling, contrast-enhanced computed tomography (CECT) showed a lytic sclerotic, multilocular mass arising from the maxilla with the presence of incomplete septae (asterisk) with mineralised matrix (Panel I: Axial bone window). Significant solid soft tissue component with enhancement greater (arrow) than the surrounding muscles was also noted (Panel II: Axial soft tissue window images). Curved MPR images (Panel III: Bone window) showed resorption of the roots (empty arrow) and floor of the nasal cavity; C: A 24-year-old woman presented with progressive jaw swelling over the last 6 mo, with intermittent pain. CECT showed a sclerotic lytic lesion with a honeycomb appearance (Panel I: Axial bone window) arising from the mandible. The lesion showed thick bony septae with mineralised matrix (asterisk). The associated soft tissue component showed enhancement similar to the surrounding muscles (orange arrow: Panel II: Axial soft tissue window). The tumour (blue arrow) can be seen encroaching onto the distal end (#) of the left inferior alveolar canal (Panel III: Curved MPR bone window).

showed both sclerotic and lytic components on the bone window, while 60% of ameloblastomas had a predominant lytic appearance (Figures 2 and 3). Additionally, the presence of osteoid either in the form of a mineralised matrix, thin bony septa or thick bony septa with dense mineralised matrix was a significant feature, and was present in 83% of CGCGs. In comparison, 70% of ameloblastomas had no mineralisation. Imaging features of ameloblastomas as contrasted with CGCGs are presented in Table 4 and Figures 2 and 3. Solid soft tissue was present in > 90% of all CGCGs, while 18% of ameloblastomas were purely lytic. The solid component of CGCGs showed avid enhancement in 50% of cases, while in the rest it showed enhancement similar to surrounding muscles, and only 4% of ameloblastomas showed hyperenhancement. On quantitative evaluation, we found that the solid components in CGCGs enhanced significantly greater than the solid tissue in ameloblastomas. Nackos *et al*[4] in their case series of seven CGCGs reported that the soft tissue in all the CGCGs showed avid contrast enhancement. Similarly, in our series, 50% of CGCGs showed enhancement greater than surrounding muscles, while the rest showed similar enhancement. While a mathematical discussion of each of the parameters used is beyond this paper's scope, briefly, entropy characterises the randomness of the distribution of the HU

Table 4 Summary of radiographic, multidetector computed tomography and magnetic resonance imaging findings in central giant cell granulomas and ameloblastomas

	Ameloblastoma	CGCG
Radiography	Posterior mandible; unilocular or multilocular; scalloped margins; root resorption, root displacement and bone expansion- may erode the cortex	Central mandible; multilocular sclerotic; root resorption, root displacement and bony expansion and cortical erosion
CBCT or MDCT	Mixed solid and cystic or purely cystic with thick enhancing rim or enhancing nodule (in unicystic variant)	Avid enhancement of soft tissue; mineralised matrix; better bony details
Our findings	Unilocular 66.7%; lytic 60.6%; solid component shows isoenhancement compared to surrounding muscles 63%; no matrix mineralisation in 69.7%	Multilocular 58.3%; mixed lytic sclerotic 75%; solid component shows hyperenhancement compared to surrounding muscles 50%; matrix mineralisation in 83.3%
MRI	T1 weighted - isointense; T2 weighted - hyperintense- cystic component; Heterogenous solid component	T1 weighted isointense; T2 weighted hyperintense to heterogeneous solid component

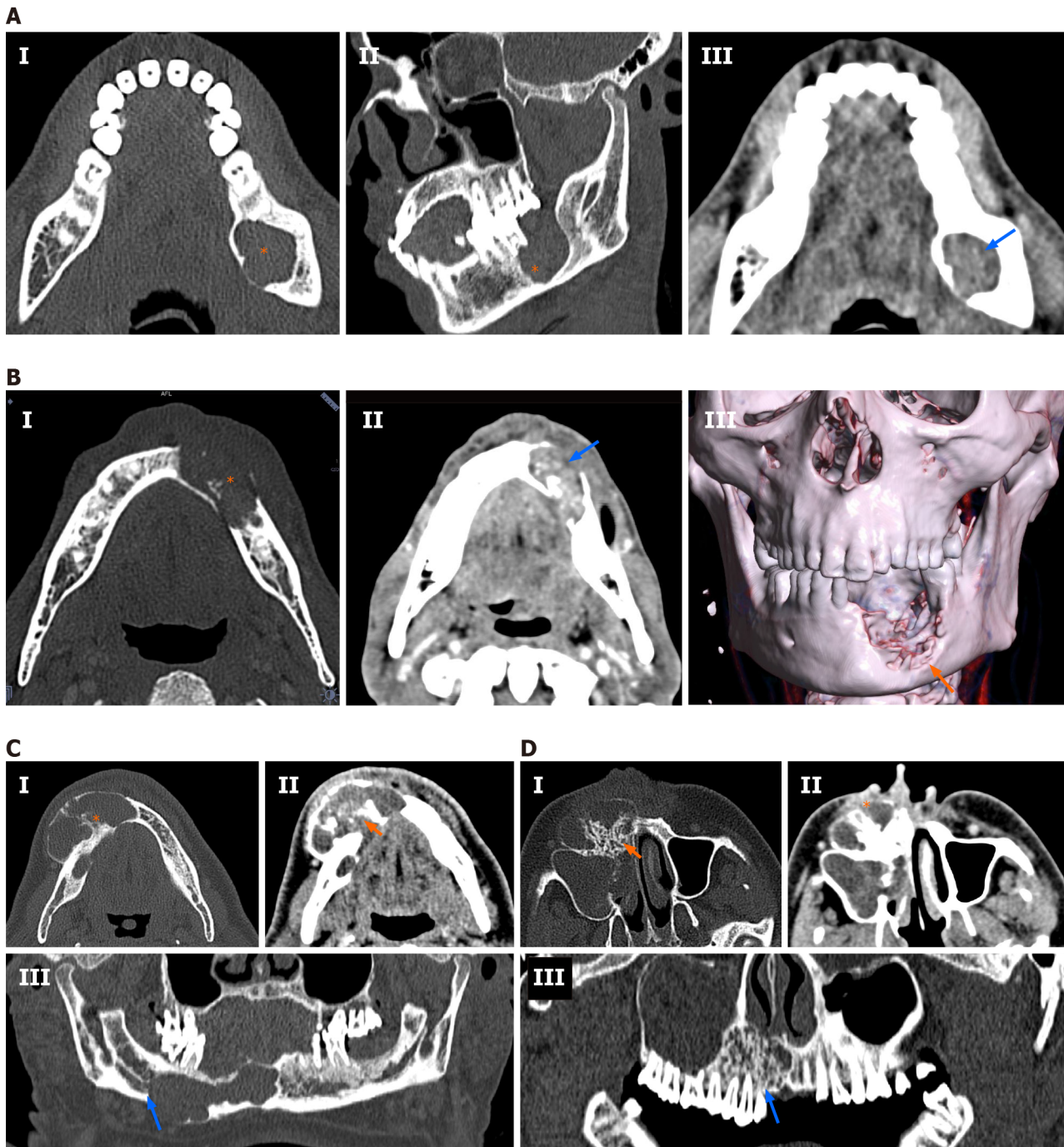
CBCT: Cone beam computed tomography; CGCG: Central giant cell granulomas; MDCT: Multidetector computed tomography; MRI: Magnetic resonance imaging.

values in the ROI. Skewness quantifies the asymmetry in the distribution of the HU values; meanwhile, kurtosis measures the histogram’s peak obtained from the HU values. A more detailed description can be read in the review by Lubner *et al*[23]. Histogram analysis showed that the mean, minimum and maximum enhancement of CGCGs was significantly higher than that of ameloblastomas (Tables 2 and 3). A cutoff > 49.05 HU for minimum enhancement in the tumour allowed 100% (63.1%-100.0%) sensitivity and 85.71% (63.7%-97.0%) specificity in differentiating CGCG from ameloblastoma.

The difference in enhancement patterns may be explained based on microvascular density (MVD) of these two tumours. While there are no studies directly comparing MVD of these two entities, separate studies have shown that ameloblastomas had an MVD of 14.9 ± 6[27] compared to 24.5 ± 5.8 in CGCGs [28]. This difference, we hypothesise, would result in a faster and a more considerable peak enhancement in CGCGs than in ameloblastomas, which would then translate to differences in the maximum and minimum venous phase-contrast enhancement of CGCGs. Orthopantomography and CBCT only evaluate the morphology of tumours. Tumour vascularity, enhancement and MVD are important components of radiological tumour assessment and can be evaluated using contrast-enhanced MDCTs. Since in an index case, morphological imaging feature may overlap, the marked differences in enhancement may allow a confident prospective distinction between CGCGs and ameloblastomas.

CGCGs are rare tumours of the jaw making their prospective diagnosis difficult. The classical lytic multilocular appearance of CGCGs on radiographs makes their differentiation difficult from odontogenic cysts, aneurysmal bone cysts, odontogenic fibromas and ameloblastomas[3,7] (the most prevalent odontogenic tumours in the developing world[9]). However, this differentiation is vital because CGCGs are treated less aggressively (curettage, intralesional interferon, steroids or calcitonin injections[8]) compared to other lesions with a similar radiological appearance. We believe this is the unique value of our study, demonstrating the utility of CECT. We acknowledge that imaging alone cannot distinguish these lesions from their other mimics, including giant cell tumours and aneurysmal bone cysts. Moreover, because CGCGs are rare, prospective radiological diagnosis is often difficult and histopathological correlation is thus needed for definitive diagnosis. Sometimes, however, a pathological diagnosis may not be forthcoming[29], and in such cases, the radiological-pathological correlation becomes essential. We believe our findings would add value in such complex cases. Moreover, in patients due to multiple concurrent CGCGs[30] in patients with a mutation of the RAS/MAPK pathway[31], or underlying systemic illnesses, not all lesions undergo biopsy. In such patients, imaging would be valuable in follow-up and diagnosis. We believe contrast-enhanced MDCT would be invaluable in work-up and management of such cases.

This study had several limitations. Of a broad potential range of lytic lesions of the jaw, we compared only ameloblastomas and CGCGs. In our routine practice, we have seen that ameloblastomas have several overlapping imaging features with CGCGs. This, compounded with the rarity of CGCGs, makes their prospective identification difficult. Given the rarity of CGCGs, we decided to contrast the imaging and enhancement characteristics of CGCGs with its most common mimic in the jaw. The retrospective design of the study, with an asymmetric dataset, might have prevented the demonstration of more variations in the imaging features of CGCGs. Because of these limitations, further prospective studies are required to investigate the imaging characteristics and enhancement features of CGCGs, ameloblastomas and their various mimics.



DOI: 10.4329/wjr.v14.i9.329 Copyright ©The Author(s) 2022.

Figure 3 Spectrum of multidetector computed tomography findings in ameloblastoma. A: A 30-year-old man presented with progressive left lower jaw swelling. Cone beam computed tomography (CBCT) showed a unilocular, lytic lesion (asterisk) with no septae involving the left angle of the mandible (Panel I and II: Axial and coronal bone window). The soft tissue component showed enhancement similar (blue arrow) to the surrounding muscles (Panel III: Axial soft tissue window); B: A 52-year-old man with lower mid jaw pain and swelling; contrast-enhanced computed tomography (CECT) showed a sclerotic, lytic multilocular lesion with thin incomplete septae (asterisk) and associated mineralised matrix (Panel I: Axial bone window). There was a significant soft tissue component showing enhancement (blue arrow) similar to the surrounding muscles (Panel II: Axial soft tissue window). Erosion of the buccal cortex was seen in three-dimensional volume-rendered images (Panel III); C: A 53-year-old man with painful progressive lower jaw swelling of 7 mo duration. CECT showed a lytic sclerotic multilocular mandibular mass with multiple thick septae (asterisk), cortical expansion and breach (Panel I: Axial bone window). The solid component present in the tumour showed hypoenhancement (arrow) compared to the surrounding muscles (Panel II: Axial soft tissue window). Hypoenhancing soft tissue was characteristically not seen in central giant cell granulomas, allowing a prospective diagnosis of ameloblastoma. Erosion of the right canal of the inferior alveolar nerve (blue arrow) was clearly seen [Panel III: Curved multiplanar coronal reconstruction (MPR), bone window]; D: A 42-year-old man with upper maxillary swelling and significant malar pain. CECT showed a lytic sclerotic mass with honeycombing (orange arrow) and thick bony septae (Panel I: Axial bone window). There was significant cortical expansion with extension into the right maxillary sinus. The mass was predominantly lytic with minimal solid component (asterisk) seen in the mass, hypoenhancing compared to the surrounding muscles (Panel II: Axial soft tissue window). Erosion of the roots (blue arrow) with honeycomb appearance was visible (Panel III: Curved MPR coronal bone window).

CONCLUSION

Significant hyperenhancement of the soft tissue component on CECT in a jaw tumour may allow a prospective diagnosis of CGCG, especially in a multilocular lytic sclerotic centrally located jaw tumour with matrix mineralisation.

ARTICLE HIGHLIGHTS

Research background

Contrast-enhanced multidetector computed tomography (MDCT) can provide unique information about ameloblastomas and central giant cell granulomas (CGCGs).

Research motivation

To evaluate contrast-enhanced multidetector computed tomography (MDCT) features of ameloblastomas and CGCGs.

Research objectives

To describe differentiating MDCT features in CGCGs and ameloblastomas and to compare the differences in the enhancement of these two lesions qualitatively and using histogram analysis.

Research methods

MDCTs of CGCGs and ameloblastomas were retrospectively reviewed to evaluate qualitative imaging descriptors. Histogram analysis was used to compare the extent of enhancement of the soft tissue. Fisher's exact test and Mann-Whitney *U* test were used for statistical analysis ($P < 0.05$).

Research results

Twelve CGCGs and 33 ameloblastomas were reviewed. Ameloblastomas had a predilection for the posterior mandible with none of the CGCGs involving the angle. CGCGs were multilocular (58.3%), with a mixed lytic sclerotic appearance (75%). Soft tissue component was present in 91% of CGCGs, which showed hyperenhancement (compared to surrounding muscles) in 50% of cases, while the remaining showed isoenhancement. Matrix mineralisation was present in 83.3% of cases. Ameloblastomas presented as a unilocular (66.7%), lytic (60.6%) masses with solid components present in 81.8% of cases. However, the solid component showed isoenhancement in 63%. No matrix mineralisation was present in 69.7% of cases. Quantitatively, the enhancement of soft tissue in CGCGs was significantly higher than in ameloblastomas on histogram analysis ($P < 0.05$), with a minimum enhancement of > 49.05 HU in the tumour, providing 100% sensitivity and 85% specificity in identifying CGCG.

Research conclusions

A multilocular, lytic sclerotic lesion with significant hyperenhancing soft tissue component, which spares the angle of the mandible and has matrix mineralisation, should indicate a prospective diagnosis of CGCG.

Research perspectives

Future studies can evaluate the role of perfusion imaging for differentiating these two tumour types.

FOOTNOTES

Author contributions: Ghosh A contributed to methodology, software; Ghosh A and Lakshmanan M contributed to writing - original draft; Lakshmanan M contributed to investigation; Bhalla AS and Manchanda S contributed to conceptualization; Bhalla AS, Manchanda S, Kumar P, Bhutia O, and Mridha AR contributed to writing - review & editing, supervision; Kumar P, Bhutia O, and Mridha AR contributed to resources.

Institutional review board statement: The study was reviewed and approved by the All India Institute of Medical Science, New Delhi Institutional Review Board [(Approval No.IEC-622/03.07.2020, RP-31/2020)].

Informed consent statement: The requirement of signed consent forms was waived by the Institutional Ethics Board.

Conflict-of-interest statement: All the authors declare that they have no conflict of interest.

Data sharing statement: No additional data are available.

Open-Access: This article is an open-access article that was selected by an in-house editor and fully peer-reviewed by external reviewers. It is distributed in accordance with the Creative Commons Attribution NonCommercial (CC BY-NC 4.0) license, which permits others to distribute, remix, adapt, build upon this work non-commercially, and license their derivative works on different terms, provided the original work is properly cited and the use is non-commercial. See: <https://creativecommons.org/licenses/by-nc/4.0/>

Country/Territory of origin: India

ORCID number: Ashu Seith Bhalla [0000-0003-2200-2544](https://orcid.org/0000-0003-2200-2544).

S-Editor: Liu JH

L-Editor: Kerr C

P-Editor: Liu JH

REFERENCES

- 1 WHO histological classification of tumours of the oral cavity and oropharynx [DOI: [10.1007/978-2-287-92246-6_11](https://doi.org/10.1007/978-2-287-92246-6_11)]
- 2 **Flanagan AM**, Speight PM. Giant cell lesions of the craniofacial bones. *Head Neck Pathol* 2014; **8**: 445-453 [PMID: [25409853](https://pubmed.ncbi.nlm.nih.gov/25409853/) DOI: [10.1007/s12105-014-0589-6](https://doi.org/10.1007/s12105-014-0589-6)]
- 3 **Etöz M**, Asantogrol F, Akyol R. Central giant cell granulomas of the jaws: retrospective radiographic analysis of 13 patients. *Oral Radiol* 2020; **36**: 60-68 [PMID: [30825099](https://pubmed.ncbi.nlm.nih.gov/30825099/) DOI: [10.1007/s11282-019-00380-7](https://doi.org/10.1007/s11282-019-00380-7)]
- 4 **Nackos JS**, Wiggins RH 3rd, Harnsberger HR. CT and MR imaging of giant cell granuloma of the craniofacial bones. *AJNR Am J Neuroradiol* 2006; **27**: 1651-1653 [PMID: [16971606](https://pubmed.ncbi.nlm.nih.gov/16971606/)]
- 5 **Abdel Razek AA**. Computed tomography and magnetic resonance imaging of maxillofacial lesions in renal osteodystrophy. *J Craniofac Surg* 2014; **25**: 1354-1357 [PMID: [24902107](https://pubmed.ncbi.nlm.nih.gov/24902107/) DOI: [10.1097/SCS.0000000000000819](https://doi.org/10.1097/SCS.0000000000000819)]
- 6 **Triantafyllidou K**, Venetis G, Karakinaris G, Iordanidis F. Central giant cell granuloma of the jaws: a clinical study of 17 cases and a review of the literature. *Ann Otol Rhinol Laryngol* 2011; **120**: 167-174 [PMID: [21510142](https://pubmed.ncbi.nlm.nih.gov/21510142/) DOI: [10.1177/000348941112000305](https://doi.org/10.1177/000348941112000305)]
- 7 **Dunfee BL**, Sakai O, Pistey R, Gohel A. Radiologic and pathologic characteristics of benign and malignant lesions of the mandible. *Radiographics* 2006; **26**: 1751-1768 [PMID: [17102048](https://pubmed.ncbi.nlm.nih.gov/17102048/) DOI: [10.1148/rg.266055189](https://doi.org/10.1148/rg.266055189)]
- 8 **Pogrel AM**. The diagnosis and management of giant cell lesions of the jaws. *Ann Maxillofac Surg* 2012; **2**: 102-106 [PMID: [23482697](https://pubmed.ncbi.nlm.nih.gov/23482697/) DOI: [10.4103/2231-0746.101325](https://doi.org/10.4103/2231-0746.101325)]
- 9 **Lasisi TJ**, Adisa AO, Olusanya AA. Appraisal of jaw swellings in a Nigerian tertiary healthcare facility. *J Clin Exp Dent* 2013; **5**: e42-e47 [PMID: [24455050](https://pubmed.ncbi.nlm.nih.gov/24455050/) DOI: [10.4317/jced.51011](https://doi.org/10.4317/jced.51011)]
- 10 **Brown NA**, Betz BL. Ameloblastoma: A Review of Recent Molecular Pathogenetic Discoveries. *Biomark Cancer* 2015; **7**: 19-24 [PMID: [26483612](https://pubmed.ncbi.nlm.nih.gov/26483612/) DOI: [10.4137/BIC.S29329](https://doi.org/10.4137/BIC.S29329)]
- 11 **Odukoya O**, Effiom OA. Clinicopathological study of 100 Nigerian cases of ameloblastoma. *Niger Postgrad Med J* 2008; **15**: 1-5 [PMID: [18408774](https://pubmed.ncbi.nlm.nih.gov/18408774/)]
- 12 **Agbaje JO**, Olumuyiwa Adisa A, Ivanova Petrova M, Adenike Olusanya A, Osayomi T, Ajibola Effiom O, Oladele Soyele O, Gbenga Omitola O, Babajide Olawuyi A, Obos Okiti R, Eziafa Saiki T, Fomete B, Aremu Ibikunle A, Okwuosa C, Abimbola Olajide M, Mofoluwake Ladeji A, Emmanuel Adebisi K, Mobola Emmanuel M, Sikiru Lawal H, Uwadia E, Oludare Fakuade B, Mohammed Abdullahi Y, Politis C. Biological profile of ameloblastoma and its location in the jaw in 1246 Nigerians. *Oral Surg Oral Med Oral Pathol Oral Radiol* 2018; **126**: 424-431 [PMID: [30126803](https://pubmed.ncbi.nlm.nih.gov/30126803/) DOI: [10.1016/j.oooo.2018.06.014](https://doi.org/10.1016/j.oooo.2018.06.014)]
- 13 **Cadavid AMH**, Araujo JP, Coutinho-Camillo CM, Bologna S, Junior CAL, Lourenço SV. Ameloblastomas: current aspects of the new WHO classification in an analysis of 136 cases. *Surg Exp Pathol* 2019 [DOI: [10.1186/s42047-019-0041-z](https://doi.org/10.1186/s42047-019-0041-z)]
- 14 **Effiom OA**, Ogundana OM, Akinshipo AO, Akintoye SO. Ameloblastoma: current etiopathological concepts and management. *Oral Dis* 2018; **24**: 307-316 [PMID: [28142213](https://pubmed.ncbi.nlm.nih.gov/28142213/) DOI: [10.1111/odi.12646](https://doi.org/10.1111/odi.12646)]
- 15 **Malignant Tumours Involving the Jaws**. In: Atlas of Oral and Maxillofacial Radiology [Internet]. Chichester, UK: John Wiley & Sons, Ltd; 2017 [DOI: [10.1002/9781118939604.ch11](https://doi.org/10.1002/9781118939604.ch11)]
- 16 **Meyer KA**, Bancroft LW, Dietrich TJ, Kransdorf MJ, Peterson JJ. Imaging characteristics of benign, malignant, and infectious jaw lesions: a pictorial review. *AJR Am J Roentgenol* 2011; **197**: W412-W421 [PMID: [21862767](https://pubmed.ncbi.nlm.nih.gov/21862767/) DOI: [10.2214/AJR.10.7225](https://doi.org/10.2214/AJR.10.7225)]
- 17 **Özgür A**, Kara E, Arpacı R, Arpacı T, Esen K, Kara T, Duce MN, Apaydın FD. Nonodontogenic mandibular lesions: differentiation based on CT attenuation. *Diagn Interv Radiol* 2014; **20**: 475-480 [PMID: [25297390](https://pubmed.ncbi.nlm.nih.gov/25297390/) DOI: [10.5152/dir.2014.14143](https://doi.org/10.5152/dir.2014.14143)]
- 18 **Hayashi K**, Tozaki M, Sugisaki M, Yoshida N, Fukuda K, Tanabe H. Dynamic multislice helical CT of ameloblastoma and odontogenic keratocyst: correlation between contrast enhancement and angiogenesis. *J Comput Assist Tomogr* 2002; **26**: 922-926 [PMID: [12488736](https://pubmed.ncbi.nlm.nih.gov/12488736/) DOI: [10.1097/00004728-200211000-00011](https://doi.org/10.1097/00004728-200211000-00011)]
- 19 **Apajalahti S**, Kelppe J, Kontio R, Hagström J. Imaging characteristics of ameloblastomas and diagnostic value of computed tomography and magnetic resonance imaging in a series of 26 patients. *Oral Surg Oral Med Oral Pathol Oral Radiol* 2015; **120**: e118-e130 [PMID: [26166034](https://pubmed.ncbi.nlm.nih.gov/26166034/) DOI: [10.1016/j.oooo.2015.05.002](https://doi.org/10.1016/j.oooo.2015.05.002)]
- 20 **Oda M**, Staziaki PV, Qureshi MM, Andreu-Arasa VC, Li B, Takumi K, Chapman MN, Wang A, Salama AR, Sakai O. Using CT texture analysis to differentiate cystic and cystic-appearing odontogenic lesions. *Eur J Radiol* 2019; **120**: 108654

- [PMID: 31539792 DOI: 10.1016/j.ejrad.2019.108654]
- 21 **Jadu FM**, Pharoah MJ, Lee L, Baker GI, Allidina A. Central giant cell granuloma of the mandibular condyle: a case report and review of the literature. *Dentomaxillofac Radiol* 2011; **40**: 60-64 [PMID: 21159917 DOI: 10.1259/dmfr/85668294]
 - 22 **Hosur MB**, Puranik RS, Vanaki SS, Puranik SR, Ingaleshwar PS. Clinicopathological profile of central giant cell granulomas: An institutional experience and study of immunohistochemistry expression of p63 in central giant cell granuloma. *J Oral Maxillofac Pathol* 2018; **22**: 173-179 [PMID: 30158768 DOI: 10.4103/jomfp.JOMFP_260_17]
 - 23 **Lubner MG**, Smith AD, Sandrasegaran K, Sahani DV, Pickhardt PJ. CT Texture Analysis: Definitions, Applications, Biologic Correlates, and Challenges. *Radiographics* 2017; **37**: 1483-1503 [PMID: 28898189 DOI: 10.1148/rg.2017170056]
 - 24 **Meng Y**, Zhao YN, Zhang YQ, Liu DG, Gao Y. Three-dimensional radiographic features of ameloblastoma and cystic lesions in the maxilla. *Dentomaxillofac Radiol* 2019; **48**: 20190066 [PMID: 31124699 DOI: 10.1259/dmfr.20190066]
 - 25 **Ariji Y**, Morita M, Katsumata A, Sugita Y, Naitoh M, Goto M, Izumi M, Kise Y, Shimozato K, Kurita K, Maeda H, Ariji E. Imaging features contributing to the diagnosis of ameloblastomas and keratocystic odontogenic tumours: logistic regression analysis. *Dentomaxillofac Radiol* 2011; **40**: 133-140 [PMID: 21346078 DOI: 10.1259/dmfr/24726112]
 - 26 **Stavropoulos F**, Katz J. Central giant cell granulomas: a systematic review of the radiographic characteristics with the addition of 20 new cases. *Dentomaxillofac Radiol* 2002; **31**: 213-217 [PMID: 12087437 DOI: 10.1038/sj.dmfr.4600700]
 - 27 **ArabSheibani M**, Seifi S, Salehinejad J, Bijani A. Expression of CD34, VEGFR3 and eosinophil density in selected odontogenic tumors- a pilot study. *J Oral Biol Craniofac Res* 2020; **10**: 367-371 [PMID: 31687323 DOI: 10.1016/j.jobcr.2019.09.003]
 - 28 **Sadri D**, Shahsavari F, Hezarkhani M, Shafizadeh M. Expression of CD34 and CD31 in Central and Peripheral Giant Cell Granulomas. *J Dent (Shiraz)* 2019; **20**: 10-15 [PMID: 30937331 DOI: 10.30476/DENTJODS.2019.44557]
 - 29 **Upadhyaya JD**, Cohen DM, Islam MN, Bhattacharyya I. Hybrid Central Odontogenic Fibroma with Giant Cell Granuloma like Lesion: A Report of Three Additional Cases and Review of the Literature. *Head Neck Pathol* 2018; **12**: 166-174 [PMID: 28785965 DOI: 10.1007/s12105-017-0845-7]
 - 30 **Edwards PC**, Fox J, Fantasia JE, Goldberg J, Kelsch RD. Bilateral central giant cell granulomas of the mandible in an 8-year-old girl with Noonan syndrome (Noonan-like/multiple giant cell lesion syndrome). *Oral Surg Oral Med Oral Pathol Oral Radiol Endod* 2005; **99**: 334-340 [PMID: 15716842 DOI: 10.1016/j.tripleo.2004.08.021]
 - 31 **van den Berg H**, Schreuder WH, de Lange J. Multiple central giant cell tumour lesions are exclusively linked to syndromes related to RAS/MAPK pathway anomalies. *Int J Oral Maxillofac Surg* 2017; **46**: 1354-1355 [PMID: 28499505 DOI: 10.1016/j.ijom.2017.04.013]



Published by **Baishideng Publishing Group Inc**
7041 Koll Center Parkway, Suite 160, Pleasanton, CA 94566, USA
Telephone: +1-925-3991568
E-mail: bpgoffice@wjgnet.com
Help Desk: <https://www.f6publishing.com/helpdesk>
<https://www.wjgnet.com>

